A Dust-Resilient Thermal Shutter Mechanism for Lunar Radiators

Andrew S. Gibson *, Olly Poyntz-Wright *, Angus Bishop *, Matthew Oldfield *, Angel Iglesias **, Fabrice Rottmeier **, Martin Humphries + and Philipp B Hager ++

Abstract

The design of an actively controlled lunar radiator must consider the effects of lunar dust on reliability and thermal performance, with protection offered to the radiator from dust obscuration being beneficial. The challenges to develop an active radiator have been undertaken, maximizing the range of operability across all possible lunar locations, with polar scenarios prioritized. Power limitations and the extreme temperature range (-150 to +120°C) have driven material and lubricant selection. Mechanism function and radiator performance are influenced by environmental conditions, including electrostatically charged regolith exposure, solar illumination, IR heating from the surface and landers or other man-made objects, as well as heat dissipation during the lunar night. An advanced breadboard lunar shutter design is described in detail, including a summary of lessons learned through validation of key mechanism elements via component testing of prototypes, analyses, and assembly of a breadboard. Overall design and heritage aspects are covered, including adaptations to achieve a dust-resilient device suitable for landers (Argonaut/EL3), rovers and long-duration lunar surface equipment/instruments. Results from component level derisking tests are presented, including sliding seal evaluation with regolith exposure, lifetime tests of axial polymeric seals and radial metallic bushings as well as cryogenic fatigue tests of polymeric flex-pivots.

Introduction

The Lunar Thermal Shutter (LTS) is a motorized, deployable cover intended for radiators mounted on lunar landers, rovers or other payloads or instrumentation used on the lunar surface. The primary functions are to provide a protective dust cover for the radiator thermal control surface and also to allow variation of the radiator performance by changing the surface area of the radiator exposed to the lunar radiative environment (which includes direct views to space). ESA requirements specify that the mounting of the shutter to the spacecraft or other platform is to be done independently from the radiator.

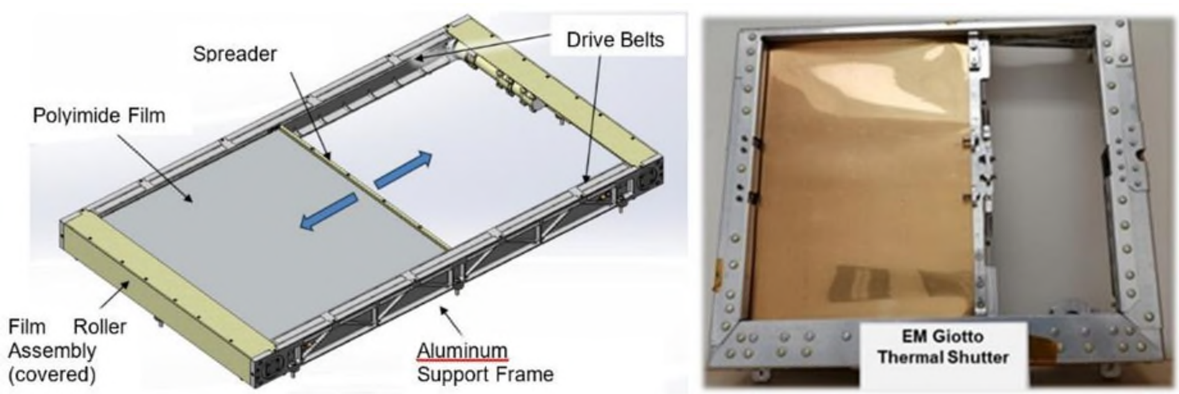

Figure 1. Left - Lunar Thermal Shutter CAD model showing spreader bar and film translation concept (external MLI covering omitted), Right - The Engineering Model Giotto Thermal Shutter [1]

* ESR Technology Limited, Warrington, UK; andrew.gibson@esrtechnology.com
** Almatech, Lausanne, Switzerland; angel.iglesias@almatech.ch
+ Spacemech Limited, Bristol, UK; martyehum52@gmail.com
++ European Space Agency (ESA/ESTEC), Noordwijk, The Netherlands; philipp.hager@esa.int

Proceedings of the 47th Aerospace Mechanisms Symposium, NASA Langley Center, May 15-17, 2024

The shutter works by deploying an aluminized polyimide film (Kapton®) over the surface of the radiator. A roller, mounted at one end of the shutter structural frame, houses a spool of film that is rolled out and in front of the radiator surface, allowing it to control the amount of exposed radiator area with a view to space.

The film roller is wound/unwound by stainless steel belts driven by sprocket wheels attached to the roller assembly. As the spool unwinds, the film is also pulled by a spreader bar that joins the two belts. The metallic belt drive system features a sealed motor/gearbox design, having a magnetic coupling at the output. This approach is intended to be more dust-resilient, having large air gaps and a lightly loaded sliding seal to prevent bulk ingress of contamination. The drivetrain is significantly different from the heritage system, avoiding the use of bevel gear configurations in the linkage and adding a magnetic coupling.

The requirement to provide active control of the louver/shutter is driven not only by the wide temperature range on the surface, but also by the presence of lunar dust, providing the ability to regulate temperature of the payload with varying dust coverage. The shutter can be opened to expose the radiator fully, partially or closed whenever necessary to provide protection, i.e., potentially during the last part of the landing, the crossing of the terminator, local activities of humans, or during activities involving movement of rovers or robotic arms.

Assembly and testing of the full mechanism, targeting TRL 4, is planned for completion by mid-2024. The status of thermal vacuum testing will be provided including characterization of heat rejection and thermal controllability vs temperature. In addition, a low-vacuum dusty test of the assembly in a new UK-based facility at the University of Glasgow is planned following thermal vacuum characterization tests.

Background

Thermal shutter and louver devices have been enabling technologies for ESA's early space exploration missions, including Giotto (Figure 1), but also for American led missions including Viking, Mariner, Cassini and Magellan and others [1,2]. These devices provide high turn-down ratios for temperature regulation of critical radiator elements of spacecraft, where cold survival, mass and reliability are critical to mission feasibility and performance. The properties that were desirable for those missions will also be key for successful thermal control on the lunar surface, where the key difference will be to work in a harsh, dusty environment, which can affect heat rejection as well as mechanism reliability.

With many projects targeting a soft landing on the lunar surface and extended operations there, thermal control challenges associated with the lunar surface environment for longer durations have become apparent related to the European Argonaut/EL3 lander as a multi-mission platform (capability to deliver mass of ~2 tons to the lunar surface by 2030). ESA selected a technology development proposal led by ESR Technology to develop a thermal control mechanism based on heritage thermal shutters from the Giotto mission to be tailored for the lunar environment and scalable across a range of sizes to maximize reuse possibilities. The development program is being performed under ESA contract, having commenced in September 2021.

An early trade-off study was performed involving 2 scalable concepts, comparing thermal louver and shutter concepts. Working model prototypes were built (incl. ½ scale shutter and 3 vane louver) to demonstrate the feasibility of both. Key features of each are summarized:

- Louver: A multi-vane adjustable angle system, mounted on dust-resilient large angle flex-pivots, driven by a single actuator system with a novel drive linkage.
- Shutter: A spooled vacuum deposited aluminum (VDA) film to adjust the view factor of the radiator surface to space, pre-tensioned and driven by a single actuator with a magnetic coupling at output to drive metal belts.

The trade-off decision making was driven by results of early thermal modelling, with the shutter option favored vs the louver concept, showing fewer scenarios with net zero radiative capacity and with potentially lower mass and higher heat rejection. The shutter was deemed simpler, having a lower part count, with the ability to protect more fully against contamination during radiation events or phases with high dust deposition, such as the passing of the day/night terminator, landing, or due to astronaut/rover/robotic activities. Shutter weaknesses were predicted for specific latitudes with the frame in vertical orientations [3] - addressed via an optional fixed baffle installed for these vertical cases, where a louvered mechanism/actuated baffle could be a preferred option for such cases. This baffle assembly is at a lower TRL, being outside the scope of the current contract.

Table 1. Summary of Key Requirements for the Dust-Resilient 'Louvered' Radiator

Parameter	Requirement Details / Values
Lifetime related Requirements	1 Earth year [goal of 2 years on lunar surface with 10,000 operation cycles (ECSS factored)], 30 krad radiation tolerance, 14 day lunar night survival implied
Thermo-Optical Properties (closed)	ϵ = IR emissivity < 0.20 (BOL) to 0.30 (EOL) α = UV absorptivity < 0.15 (EOL) to 0.25 (BOL)
Effective Radiator Properties (open)	ϵ = IR emissivity > 0.80, α =UV absorptivity < 0.20 (BOL) to 0.30 (EOL), Optical Solar Reflector or paint
Mass	Specific mass of < 9 kg/m^2 + 0.5 kg/m^2 harness = 2.05 kg (baseline size)
Scalability	Adaptable for radiator areas in the range of 0.06 to 2.0 m^2
Baseline dimensions (scalable –up/down)	Width x Length x Depth = 420 x 705 x 47 mm (shutter) = 360 x 600 mm (radiator)
Temperature Range	-150°C to +70°C (shutter operating) -150°C to +120°C (shutter survival), -223 to 120°C (surrounding surface)
Sine Vibration	15 g (17.1-100 Hz)
Random Vibration	0.25 g^2/Hz (16.7 G_{rms})
Shock	2 g at 10 Hz 2000g @ 2000-10000 Hz
Power	< 5W / m^2 = 1.08 W (baseline geometry)
Controllability	±1°C controllability (closed loop stability)

Specific requirements assert that only one actuator sub-system may be employed, limiting redundancy options to the benefit of mass/complexity. Interfaces are tailorable for mounting to aid heat transfer from heat pipe or loop heat pipe transport systems, directly to payloads or electronic boxes, etc.

Overview of Shutter Functionality, Derived Requirements & Overview of Key Mechanism Elements

Requirements for the device are summarized as shown in Table 1. The goal of the design is to have the capability to function over the widest range of locations on the lunar surface, while the temperature range specified precludes only the most extreme (shadowed) locations. Requirements to operate on the lunar surface involve difficult to simulate conditions involving charged regolith expected to be deposited fairly regularly and greater rates when the unit is located near sites of activity on the surface. This necessitates the need for dust resilience and conductive links needed to bleed charge from the film and other parts.

The requirement to provide active control of the louver/shutter was mainly driven by the presence of dust on the lunar surface and being able to regulate temperature of the payload with varying dust coverage. It was considered relevant to be able to actively open or close the louver/shutter whenever necessary, i.e., potentially during the last part of the landing, the crossing of the terminator, local activities of humans, or the movement of rovers or robotic arms.

Belt Drive and Wheel Sprocket Systems with Flex-Pivot Tensioning

The belts are driven by a motorized sprocket wheel at the opposite end of the aluminum frame. This drive wheel is attached to a stepper motor and gearhead and is driven through a non-contact magnetic coupling. When the film is deployed, the tension is maintained through a flexible element within the roller assembly. This ensures the film is deployed and recoiled in a repeatable and consistent way.

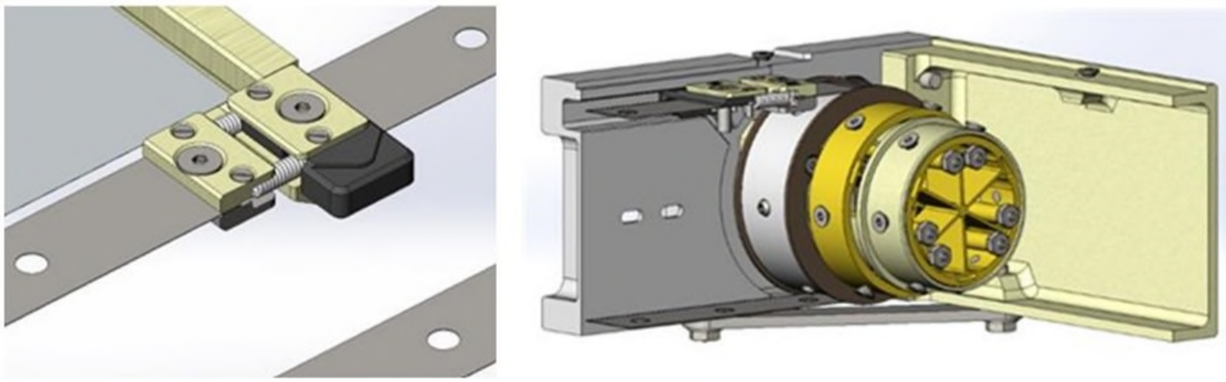

Figure 2. Spreader bar sliders and belt tensioning springs (left) and sprocket/flexure sub-assembly (right)

Flexible pivots for Roller Support and Roller Preloading

To ensure the film wraps tightly around the spool, a positive, deterministic film tension must be maintained throughout actuation. The tension in the film when fully deployed is set during assembly by deflecting the flex pivots and measuring the tension using a force gauge. As the film is retracted to expose the radiator, the thickness of film on the spool increases, and thus the radius where the film joins the spool increases. If the film is to remain taught throughout deployment, the spool must rotate relative to the wheels as the film is wound. This leads to a change in the angle of the flex pivots, and thus a change in the film tension.

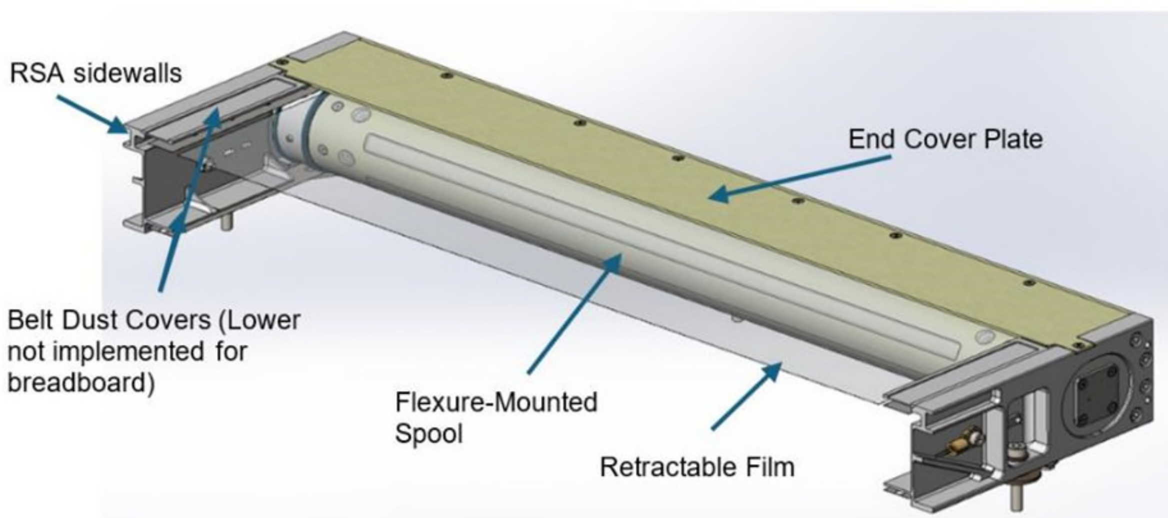

Figure 3. Roller tube film support sub-assembly

This was modelled by assuming the film forms an Archemedes spiral as it wraps around the spool, which is a useful approximation since it is a continuous function. By calculating the arc length of this spiral as a function of the wrap, the angle through which the roller must turn to entrain a given length of film can be found. Subtracting this from the angle through which the sprocket has turned gives the relative deflection angle of the flex pivots. The angle of the flex pivots, together with their spring rate and the varying spool

radius, allows the film tension to be calculated. This is illustrated in Figure 4. The minimum on this curve indicates where the radius of the film leaving the spool is exactly equal to the radius of the sprocket.
The choice of flex pivots for the spring element between the sprocket wheels and spool was driven by their dust resilience. While clock springs and bearing surfaces may have provided a lower spring rate and thus a more consistent film tension, these would have required additional tribological surfaces and accompanying dust seals. With the flex pivot design, there are no tribological components required to maintain concentricity and no geometry where sub-~0.5 mm particles could cause a seizure of the spool relative to the sprocket wheels.

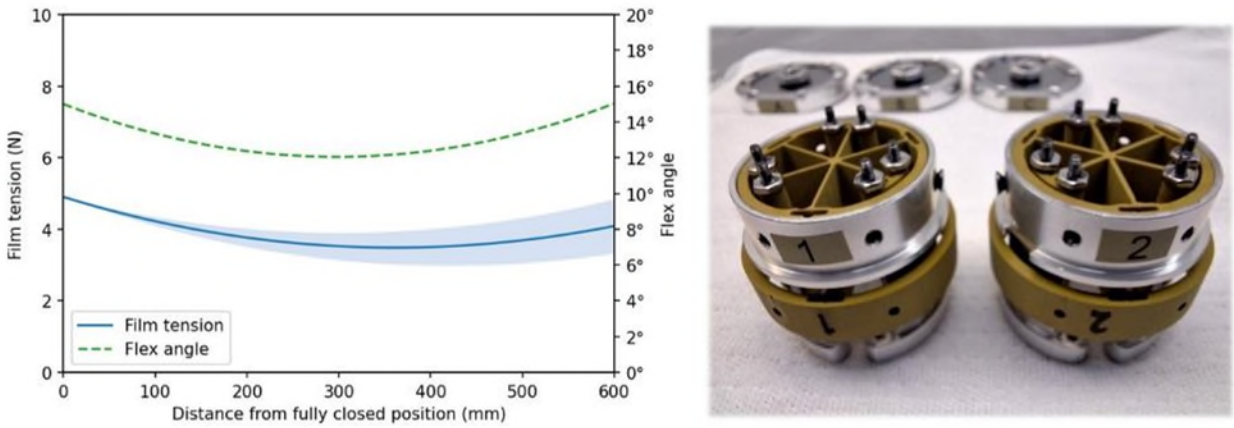

Figure 4. Left - Typical Roller Film tension and flex angle variation over actuation cycle (left) assuming tension is set in the 0-mm position (shows uncertainty bands for ±0.05-mm variation of as-machined spool diameter), dual flex pivot assembly (right) made by waterjet cutting, breadboard sub-assemblies.

Drive System with Planetary Gearhead and Magnetic Coupling Output
The drive system has been developed to meet ESA European Cooperation for Space Standardization (ECSS) requirements for torque margin in relevant environments, including on-ground with 1-g gravity (vacuum) or in vacuum under lunar gravity and incorporation of dust protection features as safeguards against this aspect of the lunar environment.

Figure 5. Magnetic coupling design and drive sub-system 'in-progress' images: Actuator test-fit with magnetic coupling inner (left), non-redundant actuator mounted in sealed housing (center), motor in sealed housing with drive wheel spigot (right)

The magnetic coupling provides torque transmission from gearhead to one wheel. The design has been optimized for this application to be mass efficient, within the specifications of actuator output stiffness and peak torque output. The deflection of the coupling is within 2 deg for expected nominal actuator operation and maximum torque transmission is approximately 1 N·m. Magnet material was selected as SmCo for consistent performance over temperature with an FeCo soft magnetic return ring and carrier used to improve the specific performance of the assembly. The magnetic coupling adds 60 g of mass to the assembly and introduces benefits including a soft launch preload and overdrive clutch (gearbox protection).

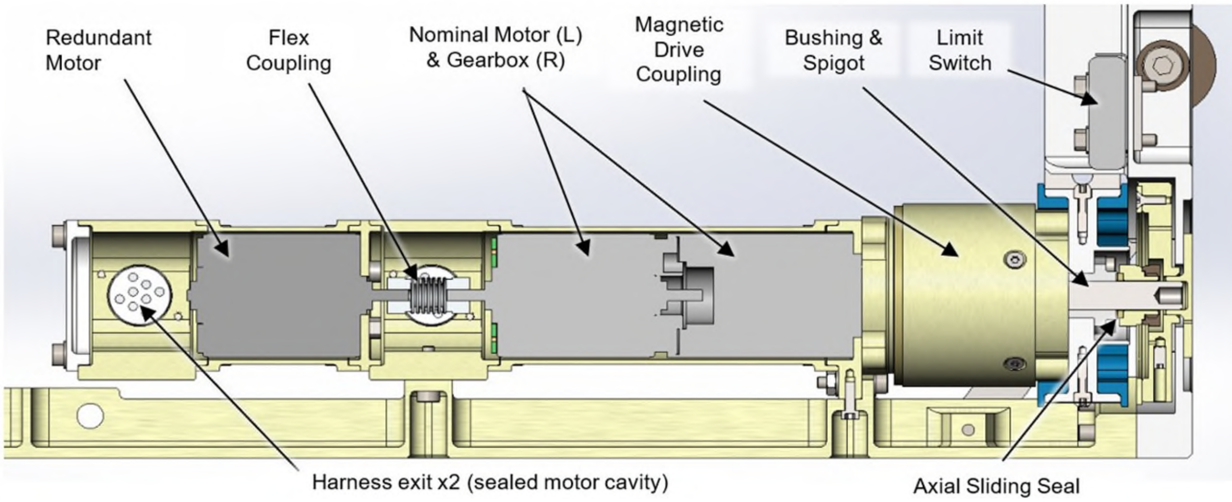

Figure 6. Actuator Drive Train (with optional redundant motor)

End Stop Limit Switches

The unit is fitted with heritage Honeywell 11HM1 switches with the JS-151 roller attachment at the end of travel in each direction, where the spreader bar triggers the roller. Redundant switches are possible as an option but not baselined given that step counting is the baseline for position knowledge, with the end stops as a secondary verification/calibration check. The effect of different shutter positions on the radiator temperature will be evaluated in the breadboard test campaign. While redundancy of intermediate position knowledge is not available, position knowledge can be reset at the end of travel.

Tribological Design Overview

Notably, the use of large-angle flex pivot technology patented by Almatech (with support from Spacemech) has limited the number of tribological contacts from the outset. These flexures ensure that the movement required for tensioning of the film on the roller will be extremely resilient to dust. This leaves the following essential tribological elements of the mechanism, consisting of:

- Motor and gearhead (quantity 1, where a redundant motor is optional)
- Sliders at ends of spreader bar (quantity 1)
- Corner support bushings (quantity 4)
- Belt to wheel sprocket interfaces (quantity 4, including 6 timing pins each and flat contacts)

Motor and Gearhead Tribology

The motor and gearhead bearings and gears have been manufactured with solid lubricant MoS_2-202 sputtered by the European Space Tribology Lab, with the intent to provide a maximum temperature range of operation without the limitation ((as is common) to heat prior to operation. This enables compliance with the ~1 W power requirement and provides maximum logistical simplicity for use across future missions. Notably, this actuator has previously been developed to TRL 6 by Almatech under ESA funding for a liquid lubricated configuration [4], while it has not been life tested for this application. The requirement on motor lifetime is seen to be challenging, with a factored demand of 7.2 million motor revolutions, but it is noted that the current program will only provide an initial derisking involving a total of approximately 30% of the intended worst-case factored lifetime. This is noted as a residual risk for future work, being deemed a lower priority in comparison with other tribological aspects being verified in this activity, as agreed with ESA.

Spreader Bar Sliders

A composite material based on Polyetheretherketone (PEEK), with a carbon filler and tribo-additives has been selected for the sliders, which are lightly loaded, flat contacts (notionally). This material has a low CTE below 30 ppm/°C and was verified to perform well in a pin-on-disc tribometer trial between -80°C and 80°C, demonstrating relatively consistent and low friction coefficient in both air and vacuum, with reasonable wear rates considering the carbon content. A small amount of wear product can be expected, which will be evaluated for acceptability at the end of test.

Corner Wheel Bushing Supports and Spigots

The wheel bushings are designed in X65Cr13 stainless steel running against spigots made of medium alloyed tool steel, both coated with sputtered MoS_2-202 deposited by ESTL. Originally, a bronze material with reduced lead content (<4% in line with transitional Restriction of Hazardous Substances (RoHC) guidance) was trialed, running against a Kolsterised® 300 series stainless steel spigot (for CTE match). This material was evaluated in the component prototype tests and was not successful, lasting on the order of a few hundred rotations. The MoS_2 coating rapidly degraded along the single line contact of the spigot. More information is provided in the prototype derisk section below. Changing the bushing to stainless steel allowed the internal diameter of the bushing to be coated with MoS_2, providing some additional resupply/recirculation of the lubricant. Additionally, the use of harder surfaces and changes to the geometry (removal of sharp edges) limited debris generation, as was seen to accelerate wear in earlier testing with bronze bushings.

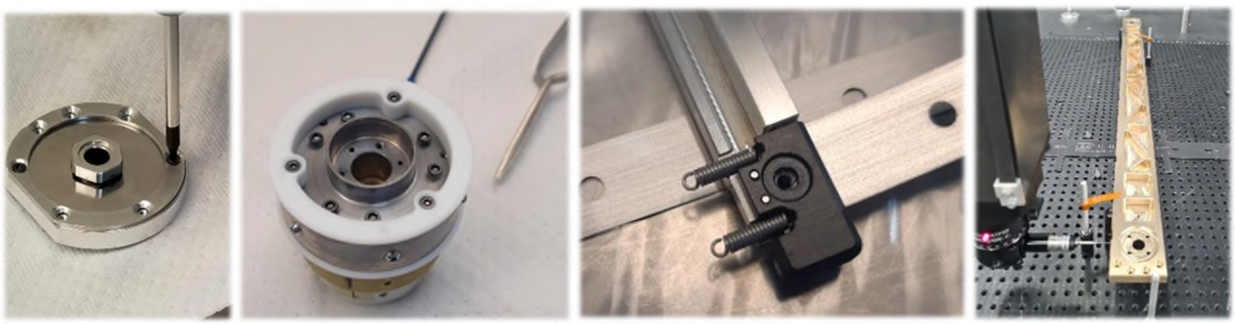

Figure 7. Breadboard Component Photos: Diaphragm spring pack (left), sprocket wheel/flex assembly (center left), spreader bar slider (center right), sidewall structure in final inspection (right)

Sliding Seals for Bushing and Magnetic Coupling protection

The axial bushing and magnetic coupling both employ lightly loaded polymeric seals to prevent significant ingress of regolith from affecting functionality. These seals are closely controlled to maintain preload of a few Newtons on bushing seals and a lighter preload on the larger magnetic coupling seal (being less sensitive with large air gaps). The sliding seal material is a composite with PolyTetraFluoroEthylene (PTFE) additive, selected from the ESTL test database having been tested in pin-on-disc tests and shown to have one of the lowest rates of wear debris generation measured, with relatively consistent friction in air and vacuum (μ = 0.1 to 0.25). The geometry of the coupling seal was optimized following early dusty test trials described below.

Belts and Wheel Sprockets

The wheel hubs are made from RSA aluminum for mass savings and CTE matched to belts and will be coated with silver as a baseline (not included for breadboard). Drive pins were upgraded to PH 15-5 alloy for greater resilience versus carbon steel used in early trials. Belts are made from high yield 301 stainless steel (consistent with heritage from a previous boom mechanism) with laser cut hole patterns.

Risk Reduction by Prototype Validation

Three significant prototype initiatives were undertaken to derisk the design, two of which were tribologically focused and one focused on a fatigue check of the polymeric flexures at cryogenic temperatures.

Dusty Testing of Sliding Seals in Ambient conditions

Dust susceptibility tests were performed to examine the resilience and effectiveness of the sealing elements within the actuation train to prevent the ingress of dust. A key part of the test was to verify the selection of the preload within the sealing elements as well as the functioning of the seal geometry on the spigot and the magnetic coupling seal. The tests were intended to provide confidence in the ability of critical components to withstand exposure to lunar dust; the test methodology is not consistent however with allowing conclusions to be drawn on the spatial distribution of dusty material.

The dust test rig consisted of representative elements of the magnetic coupling and stub axle assembly, with a measurement of the combined resistive torque elements of the magnetic seal and the stub axle bushing and seal. The overall test setup is shown in Figure 8, which made use of several 3D-printed parts and a Commercial off-the-shelf (COTS) idler bearing assembly. Dust injection was done with Exolith LHS-1D simulant, to aim at a specific region with a flexible nozzle, with the sample released by means of a charged sample container vented into the chamber using a timed solenoid device. Torques were measured using a Kistler torque transducer by rotating the assembly in each direction for 4 revs; the reported torque value is calculated by halving the difference between the torques in each direction.

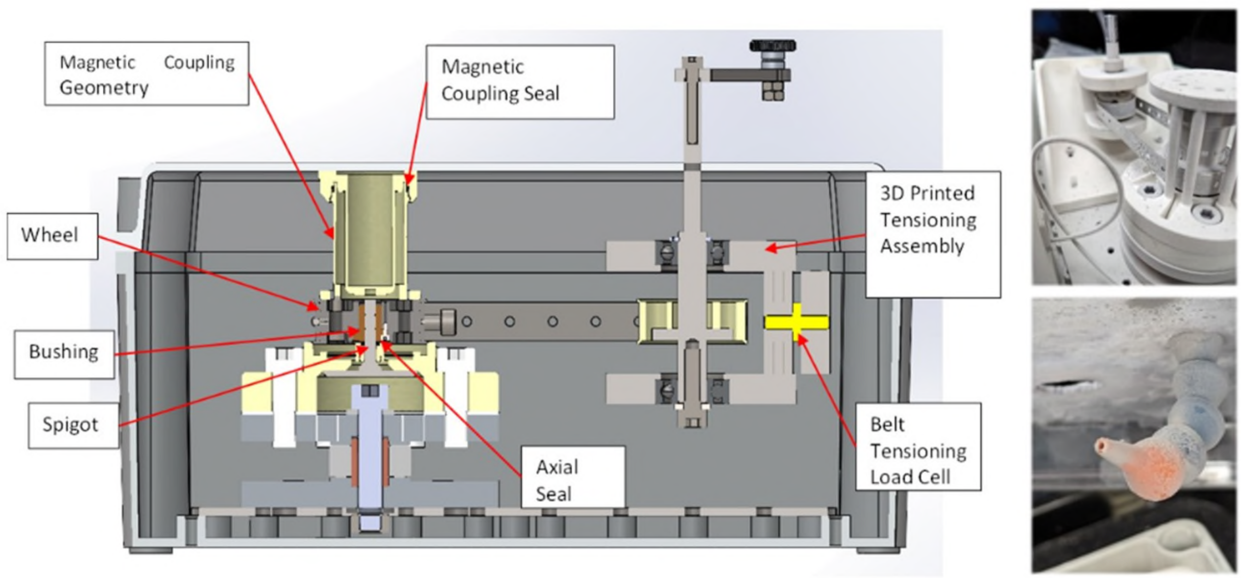

Figure 8. Ambient Dusty Test Setup with hand-cranked belt drive: CAD section view (left), view with cover removed (upper right), dust injection port (lower right)

Torque was seen to rise initially but stabilized at levels just less than double the pre-dust torque indicating some impact from the regolith interacting with seals and possibly belt to wheel interactions, but it stabilized relatively quickly following the initial increase. This indicates some room for improvement in the seals (Figure 9), though it was deemed to be a 'worst-case' test with very fine simulant in high quantity.

Bushing and Seal Prototype Lifetime Testing

Not only are the bushings required to maintain alignment and handle loads transmitted through the wheels, but these sliding contacts also need to be able to bleed charge from any significant build-up of electrostatic effects of floating elements.

A combined prototype activity was devised with the intention to validate both axial seals and radial bushings, with monitoring of radial bushing conductivity throughout. As circumstances progressed, the activities ended up with separate validations of each. An initial lack of success with a bronze bushing design being short-lived through several trials (see Figure 10), was combined with the successful verification of the associated axial seal test. This was then continued to validate the lifetime of the axial seal on its own. Despite significant debris generated internally, the soft polymeric seals continued to function and remained intact. After the bronze bushing configuration was abandoned, the axial seals were allowed to resume testing (radial load reduced) and completed prototype life-testing in vacuum.

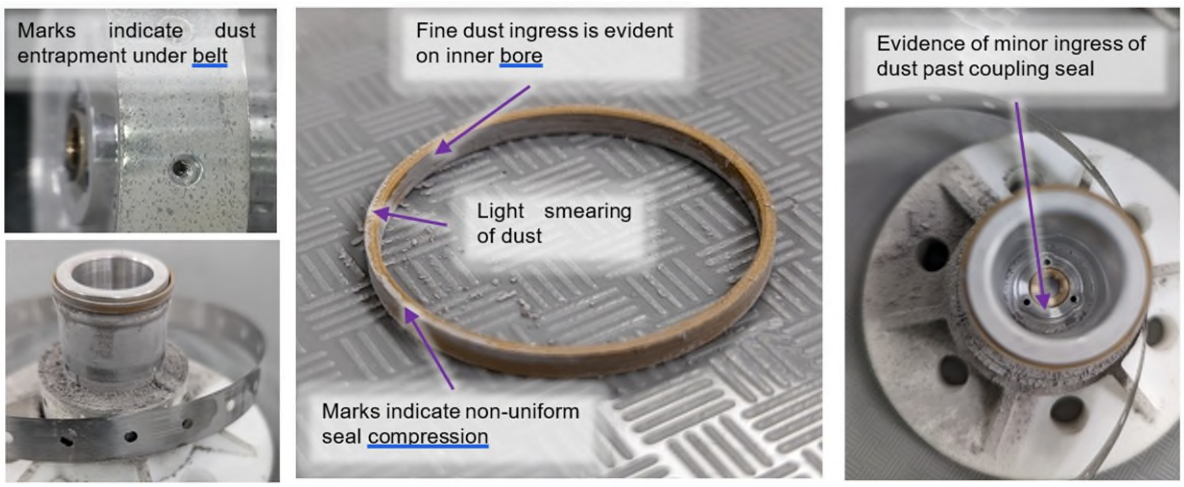

Figure 9. Dusty Test Post-Test Inspection Key Findings indicating non-ideal coupling seal function with extreme exposure to LHS-1D Exolith highland simulant (axial seals were fully successful to limit ingress)

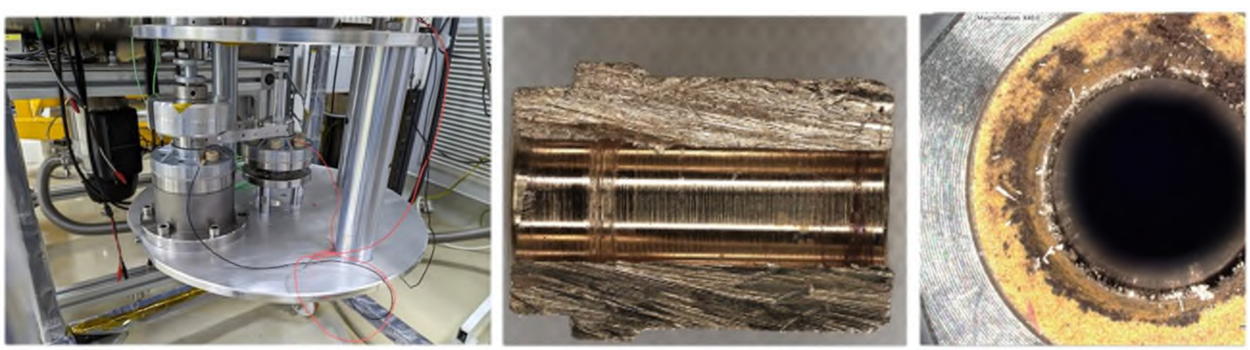

Figure 10. Vacuum test rig for bushing and axial seal evaluation (left), early bronze bushing failure (center), axial seal after 10,000 revs in air (right) with some bronze debris embedded at inner interface

In parallel, the bushing design was modified to use harder contact materials, based on an insightful study of vacuum bushings by the US Air Force [5] which described a similar, successful configuration using hardened stainless materials and sputtered MoS_2. The original design was far too dependent on the line contact with the spigot, where the MoS_2 wore away after some hundreds of rotations exposing the hardened spigot (via Kolsterising®) to run against bare bronze (with inadequate lead content to form a lubricating film) only to be worn quickly, generating significant debris. The reconfigured bushing and spigot were initially tested in air for over 8,000 revolutions followed by 19,000 in vacuum. With a 50% rise in torque observed after 14,000 cycles in vacuum, it was determined that the initial in air running had been excessive.

While the test was not intended to run so long in air, a setup error for the test led to the findings for extended run-in in air, as summarized in Figure 11. The effect of a long run-in in air demonstrates a steady increase in running torque, indicative of increased MoS_2 wear whilst the MoS_2 is known to perform less ideally in a moist environment so is not in itself surprising.

The findings emphasized the need to set a clear allocation on ground operations to avoid impacting the remaining in-vacuum lifetime and so that subsequent tests could be performed and account for a reasonable budget for in-air operation. This was set and agreed with the client to be based on 15 mechanism actuation cycles in air, where further ground testing could be performed in air or N_2 with much reduced impact. This allocation will be reviewed again ahead of qualification activities, where any inputs from potential users would be welcomed.

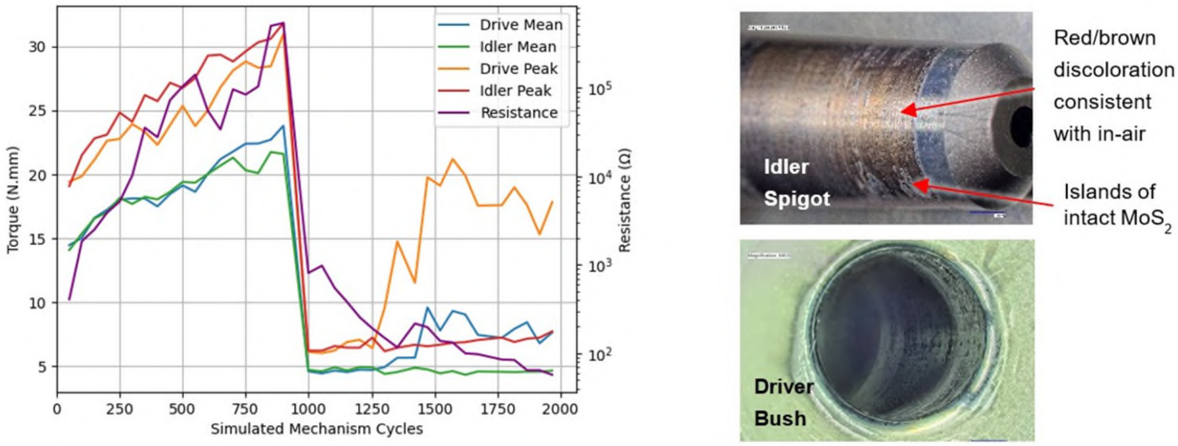

Figure 11. Preliminary Testing of Bushing/Seal Friction Torque with significant in-air run-in with reconfigured hardened steel bush and spigots with sputtered MoS_2-202 (multiply cycles x 10 for revolutions)

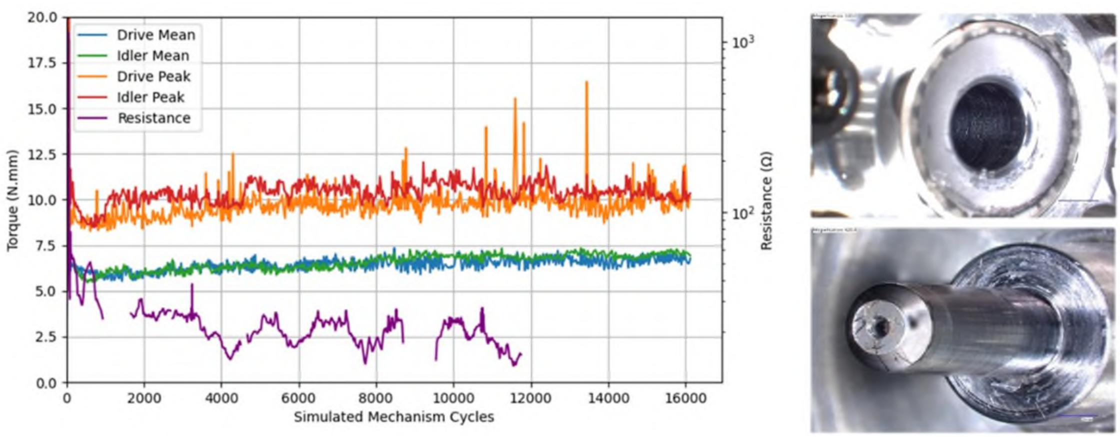

Figure 12. Left - Final prototype life testing of bushing/seal friction torque and conductance over 100,000 revolutions with hardened steel bushings and spigots with sputtered MoS_2-202, Right - Final condition of spigot and bushing following life-test protype completion (seals used were PTFE)

The bushings both demonstrated some minor surface pitting, and the spigots showed evidence of some MoS_2 degradation on the running surface. MoS_2 was still present in the bushing and on the surface of the spigots. This is indicative of an end-of-life condition for the contact.

<u>Cryogenic Prototype Testing of Polymeric Flexures for Fatigue Resilience</u>

The idea of relying on stressed polymer flexures down to the cold survival temperature of -150°C seems at first questionable, as most plastics would be highly brittle at these temperatures. However, extensive manufacturer data for the grade of Polyamide-imide used suggested that this was in fact feasible. To validate this assumption, a simple rig was designed which would allow the torque across the flexure to be measured at both at room temperature and at -150°C. This temperature was achieved by cooling a fixture at one end with LN_2 and allowing the opposite end to interact convectively with the surrounding atmosphere of dry nitrogen.

An extract of the torque data from the room temperature tests is shown in Figure 13. The material clearly exhibits some viscoelastic behavior, with decay in torque magnitude over time. This behavior was distinct from charge amplifier drift, which was expected while using a piezoelectric transducer. In the mechanism, the flexures will be deflected at a much slower rate, such that any transient effects are expected to be negligible. The 'steady state' torque was measured and compared for a range of deflection angles to fully characterize the pivot over its operating range, showing reasonable correlation with Finite Element Analysis.

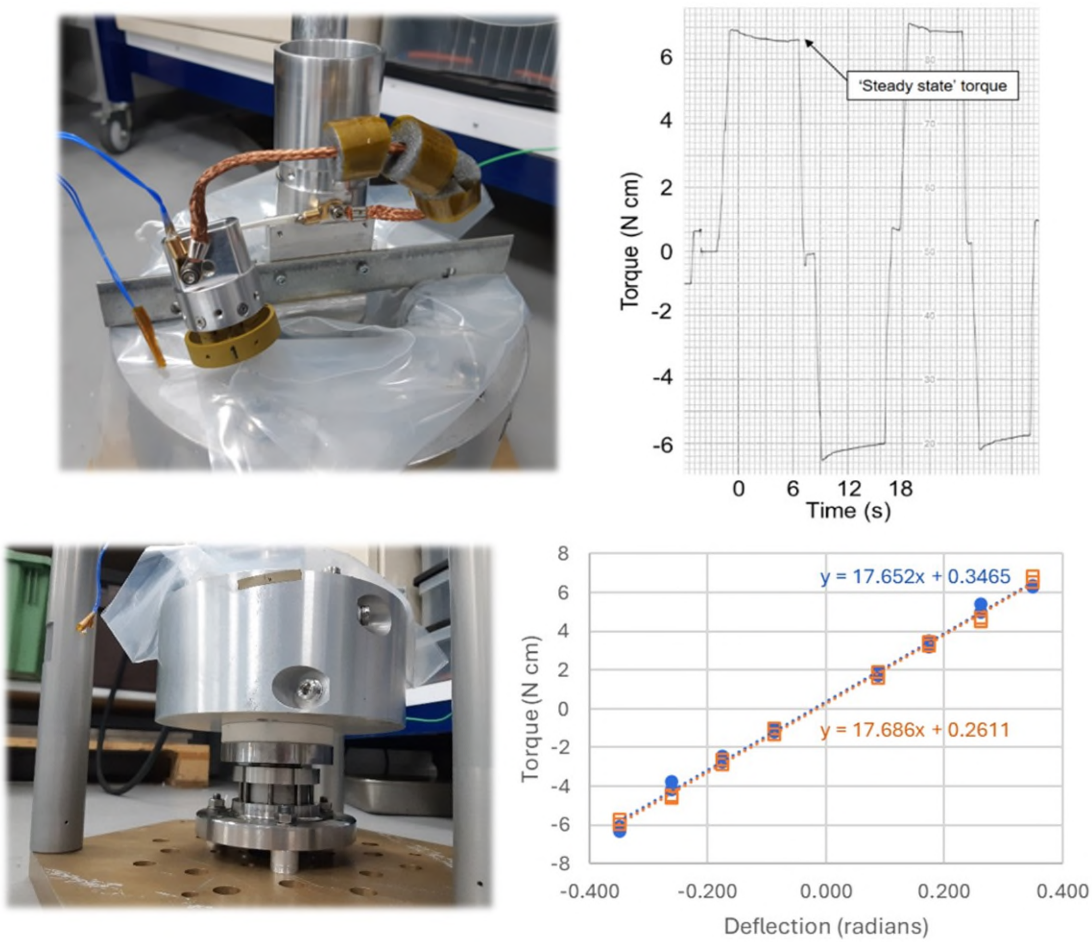

Figure 13. Cryogenic flexure test setup and results – Top Left: Flexure mounted in the large central tube, cooled via the bath at the base filled with LN_2, Top right: Torque data, showing viscoelastic behavior of the flex pivot, Bottom left: LN_2 bath mounting to Kistler Load Cell, Bottom Right: Torsional stiffness relationship checked for stability at two points during test.

These tests were repeated at -150°C with the pivot surviving over 300 cycles over its normal operating angles, with stiffness increasing at cold (factor of ~2.2). These cycles, together with over 1700 cycles at room temperature, demonstrated survival after >20% of the required lifetime. A post-test inspection confirmed no signs of damage or wear and validated these parts for use in the full mechanism build.

Structural and Thermal Considerations

A detailed thermal analysis of the LTS was performed by Almatech, considering the potential use cases of the LTS for a wide range of landing sites across the lunar surface from equator to poles. Analyses performed assumed the shutter frame external surfaces to be wrapped in MLI. For the purposes of modelling, a 10-layer blanket was assumed with a Beta-cloth external layer, although not a critical parameter and expected to be mission specific. Due to the proximity of moving parts (belts and film), MLI was only applied to external surfaces, leaving a view factor to the inside of the frame at acute angles of incidence.

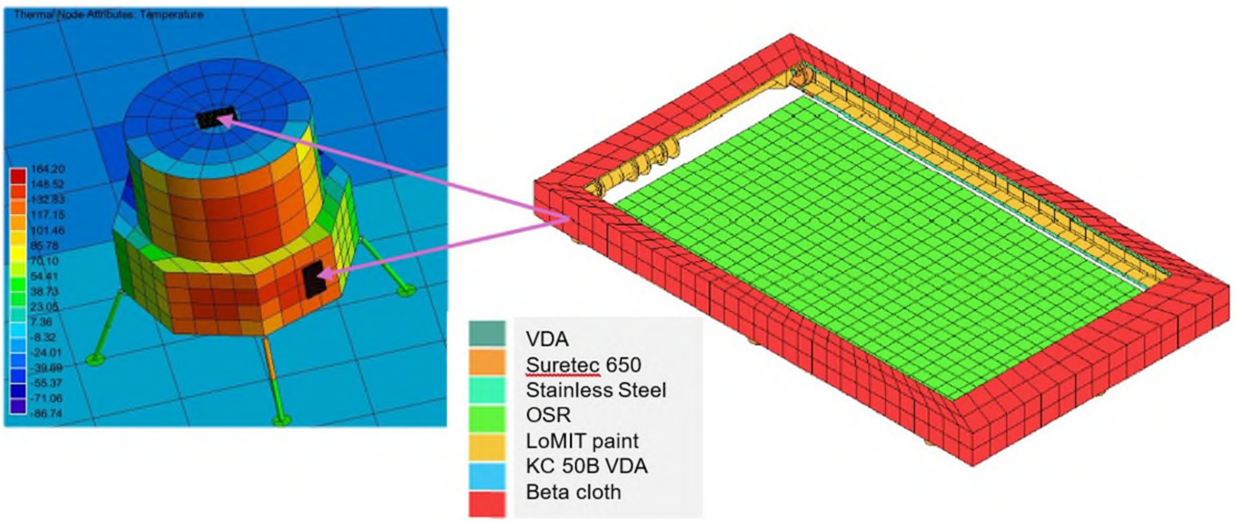

Figure 14. Thermal Case Description showing thermo-optical materials used in modeling and horizontal and vertical positioning of the shutter on the ESA generic Argonaut lander model (rover case not depicted)

With the potential for solar loading, lunar IR or albedo heat flux, the thermal finish of the inside of the frame is an important consideration. To achieve a design that is as insensitive to these heat fluxes as possible, a low emissivity (ε) and low absorptivity (α) surface finish is desirable, where a ratio of $\alpha/\varepsilon < 0.5$ is preferred to avoid a net heating effect. As part of this program of work, thermo-optical properties of Lo/MIT paint and a thin layer of Keronite® are being evaluated. The breadboard model has not been coated with these finishes along with a reference chromate coating, while the results of the thermo-optical testing on sample coupons will inform the final design choices for future iterations, where correlation modeling will be used to evaluate the effect of changes from the chromate coating on the breadboard to each of these options.

In summary, the thermal analysis predicted that the mechanical parts of the shutter would all remain within acceptable temperature limits. Estimates for the shutter thermal performance in terms of turndown ratio ranged from around a factor of 10 in the vertical orientation up to a factor of 30 for horizontal cases, in line with expectations. The thermal environment and associated temperature predictions confirmed the wide operational and non-operational temperatures that are required from the LTS with gradient predictions to be cross-checked in test.

With MoS_2 lubricant employed and materials selected to withstand the thermal environment, the main impact of the wide temperature range relates to thermo-elastic issues and the relative geometric changes in materials with different thermal expansion coefficients within the shutter. A key aspect here is maintaining the tension within the drive belts across the temperature range. If perfectly matched CTEs were possible for the drive belts and the structure and gradients limited, the belt tension would be invariant with temperature. Commonly used structural Al alloys (6000 series) have a CTE ~7 ppm/°C greater than the stainless steel belts; their use would result in near total loss of tension in the coldest cases and greatly increased tension in the warmest; both of which could render the mechanism undriveable. Therefore, a material was sought with a thermal expansion coefficient closely matched to that of stainless steel. The alloy selected was RSA-4062-T6, a proprietary alloy manufactured by RSP with a CTE that is within 0.1 ppm/°C of the stainless belts, resulting in a predicted belt tension variation of less than 0.5 N from the room temperature value.

This breadboard program seeks to verify the functionality of the LTS mechanism and to characterize the potential thermal performance in terms of heat rejection control. To demonstrate this, a custom test facility has been developed that will subject the LTS to the thermal extremes for functional testing and will also provide a representative radiative environment to gauge the effectiveness of the device as a thermal control device. For functional testing the shutter temperature is driven by heaters to above ambient temperature and utilizes a cryocooler and thermal straps for below ambient tests.

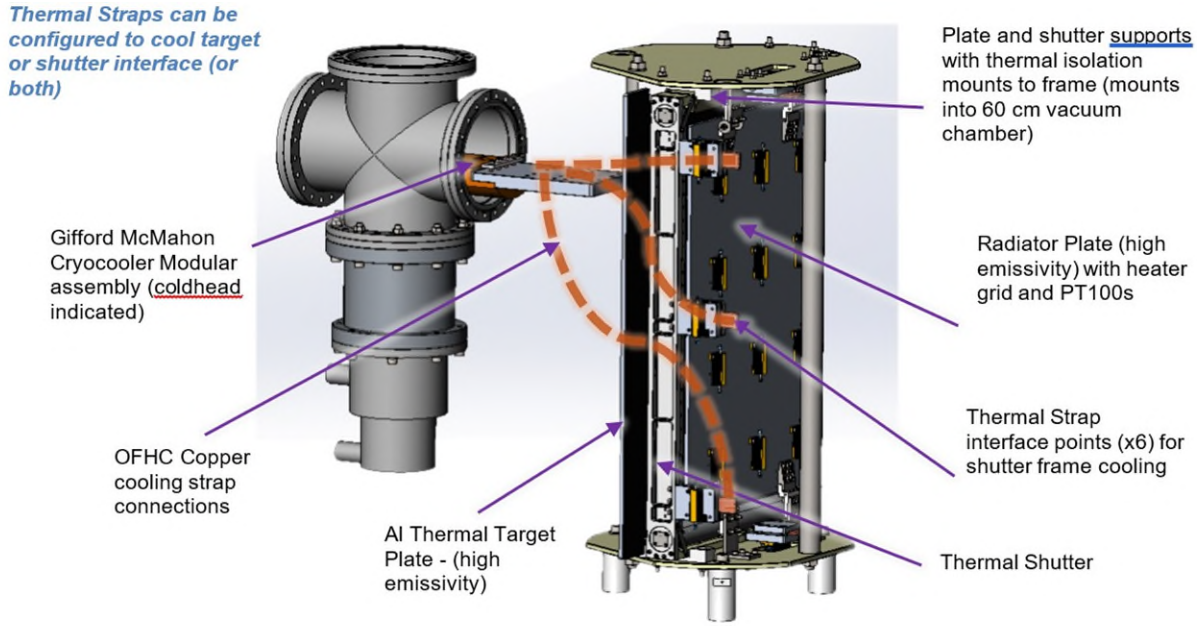

Figure 15. Thermal Vacuum Characterization Setup (60-cm diameter chamber not shown)

To assess the thermal control aspects, the shutter frame is centered around a high emissivity radiator panel, intended to be representative of a lunar lander radiator. Positioned immediately in front of the shutter is a cold target that mimics the cold radiative environment of space. This arrangement allows for the radiator to be maintained at fixed temperature whilst the power required to heat it is measured by the facility; the variance in heater power for different shutter positions will establish how much heat is being radiated to the cold target. This will allow an initial estimate of the turndown ratio the shutter could provide.

A structural analysis was also performed by Almatech to evaluate modal behavior, stresses, and loads within the shutter during launch. Some higher stressed components were found but no significant issues were identified, with adjustments made to reduce stresses. The final analysis confirmed that the expected loads on the motor and gearbox assembly were consistent with the levels already achieved during the actuator level qualification tests. Analyses also confirmed the selection of displacement limiting snubbing surfaces within the mechanism.

Lessons Learned from Prototyping and Recent Build Activities

A significant number of lessons have been learned through the design, analysis, prototyping and build activities to date, noting that the next few months of testing will undoubtedly result in further lessons learned. To date the following lessons were most notable, where the results stress the value of early, environmentally representative tests were helpful to quickly illuminate design flaws and material related issues. Errors made in testing can sometimes produce some very interesting results, in this case results were very insightful for understanding of the tribological limitations. In this case, the importance of assigning allocations for ambient testing of solid lubricated parts was emphasized early enough to plan and communicate adequately with the client.

The axial seal material, chosen for its low wear rate, was proven to be a solid choice, confirmed by testing at ambient (air & vacuum) with no issues reported. This material showed very little degradation through prototype life tests, with minimal wear products, though non-zero. This experience also highlighted the value of the ESTL database of pin-on-disc studies for tribo-material selection for new applications. Though undesirable, the bronze debris generated in early prototype testing was embedded near the inner diameter of the seals, but caused no significant issues, indicating significant resilience to the presence of debris.

The control of light preloads on axial seals has not been a trivial matter. Precise control was enabled for prototype testing with the use of fixed masses working under gravity, but to realize this in all orientations with respect to gravity in the mechanism has been more difficult. The diaphragm approach taken with steel diaphragms is an elegant solution but has resulted in a spring system with a low range of operation, of less than 300 µm which does not allow for much tolerance variation due to individual parts and necessitates some iteration in the build. The approach taken to use an uninterrupted diaphragm (no spirals etc.) was applied because of the need to block ingress of dust into the wheel system, but the solution is somewhat over-constrained. An alternative solution with a titanium diaphragm or a soft wave-washer and a polymer membrane will be considered in the future to relax tolerances.

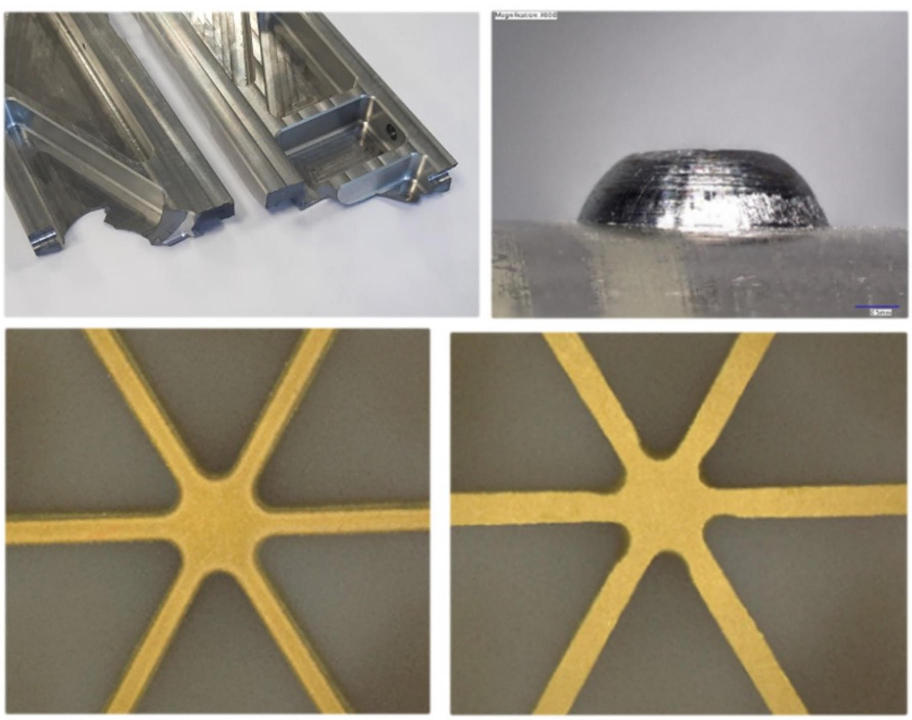

Figure 16. Materials Lessons - Brittle fracture of DISPAL S260 frame (top left), prototype timing screw wear of Ni plated carbon steel (top right), geometry variation at entry/exit of waterjet features (lower)

Early dust testing and bushing lifetime tests highlighted the sensitivity of the timing pin height and radius, identifying a non-conformance that had been missed at incoming inspection. Following this issue, tolerances were refined and adjusted to limit such issues in the future. The nickel-plated carbon steel was also deemed not hard enough based on wear observed in prototype tests, opting to change to PH 15-5 stainless. Refer to Figure 16 showing evidence of wear on this low-cost plated prototype part.

Waterjet cutting was used to manufacture the PAI flex pivot components. This allowed cutting of fairly precise flexure beams to achieve reasonable control of relative motion between parts. However, a closer inspection (as shown in Figure 16) revealed that where the water jet entered the parts, edges were clean, while opposite side edges were uneven. A draft angle was present, with the parts thicker on the jet exit side. Around the thin webs (which act as torsion springs), thickness variations of about ±15% were observed. It was also noted that the flat PAI stock had a ~1mm outer layer with a darker color than the bulk material (a product of the annealing process). While datasheets suggested this layer had the same mechanical properties as the bulk material, it proved to be harder and difficult to waterjet cut and so was milled from both sides before cutting. The worst-case effects on stresses will require some further consideration, to establish appropriate controls prior to qualification.

A substitute material used for the breadboard frame, aimed at reducing cost and schedule, while maintaining realistic CTE effects, was problematic. DISPAL S260 was selected to have a representative CTE (within 0.5 ppm/°C) of the baseline alloy (RSA 4062-T6) but resulted in machining difficulties. While the materials have a similar composition featuring high silicon content, the DISPAL was considerably more brittle, with elongation of about 0.5% vs 2.5% for the baseline RSA material. Two failures of parts occurred near to completion of machining deep pockets in the sidewall parts. One part was made successfully, given several stress relief cycles, while the mirror image part was never completed, despite procuring additional material and near identical geometry. As a compromise, one breadboard wall was made from a bronze alloy with a similar CTE, accepting a mass difference for this build. In addition to brittle behavior, symmetric pocket design (on either side of the wall) would have been beneficial to balance stresses, or to opt for Electrical Discharge Machining to avoid stress accumulation.

Early prototyping work allowed for rapid validation of magnetic concepts. Producing custom magnets and soft magnetic materials requires a good relationship with a magnet vendor, but when this is in place model validation can be inexpensive and fast. Use of early motorisation margin targets as design requirements, with envelope limitations applied, produced a good set of constraints for iteration. Stiffness, peak torque, size, mass, and ease of assembly are competing requirements, but automated analysis and processing helped, and the results provided confidence that solutions were feasible.

The timing/wide scope of a proposed fluorinated product ban in the EU, which emerged at the commencement of the program, poses potential issues going forward that will require consideration. Prior awareness might have affected material selections and could require considerable additional testing in the future.

Conclusions

The design of a lunar thermal shutter has been significantly advanced and derisked to overcome various environmental and lifetime challenges posed, including for wide thermal limits and a dusty lunar environment, such that it can be expected to be suitable for a wide range of payload/lander/rover applications. A full test campaign is planned to be completed in the upcoming months to further verify the capability of the full mechanism design to operate in these environments.

Extensive component testing has been performed to verify the suitability of the bushing and seal technologies, in terms of lifetime and conductivity to bleed charge from the assembly. Axial seals showed the required durability to protect from lunar dust and to meet the required lifetime but will require testing in higher fidelity lunar simulation environments to be able to declare them fully resilient and compatible with electrostatic challenges for a range of missions. The program of work has also proven the potential for long lifetimes of dust-resilient polymeric flex pivots for small angle oscillations, operating to cryogenic temperatures. Further it has been demonstrated that the electrical connection through sliding metallic bushings, with sputtered MoS_2 lubrication, can be maintained consistently throughout the required lifetime, with relatively low resistance maintained and trending lower throughout the lifetime.

Clearly, further adaptations may be required to enhance dust resilience of the mechanism following upcoming evaluations in dusty low vacuum testing, where lessons learned with this technology for radiators should be transferrable to other lunar applications involving solar panels, which share a similar susceptibility to dust. The device can also be considered for use as solar habitat solar blinds, particularly given scalability and relative ease of adaptation to different platforms. The importance of this type of thermal control in various lunar surface applications, with dust protection incorporated to ensure reliable operation, should not be underestimated. However, the design will require further work to mitigate the effects of lunar regolith in increasingly realistic environmental tests, to ensure the effectiveness for the future success of landers, rovers and other payload performances in more extreme environments and to survive the lunar night.

References

1. Felici, F., Brouwer, G.F., "The Giotto Thermal Control Shutter," *13th ICES Proceedings*, San Francisco (1983), 337-344.
2. Gilmore, D. G., *Spacecraft Thermal Control Handbook: Volume 1: Fundamental Technologies*, 2nd Edition, Chapter 9 (Louvers), El Segundo, California, AIAA - Aerospace Press ©2002.
3. Gibson, A.S., Bailes-Brown, D. et al, "Design of an Actively Shuttered Dust-Resilient Radiator for Lunar Applications", 52nd ICES, Calgary, Canada, ICES-2023-448 (2023).
4. Hayoz, S., Blecha, L., Liberatoscioli, S., Rottmeier, F. et al, "Miniaturised Stepper Motor for Space Applications", 19th European Space Mechanisms and Tribology Symposium (2021).
5. Rachel S. Colbert, Luis A. Alvarez, Matthew A. Hamilton, et al, "Edges, clearances, and wear: Little things that make big differences in bushing friction", Wear 268 (2010) 41-49.